


Probing the in-plane electron spin polarization in Ge/Si_{0.15}Ge_{0.85} multiple quantum wells

C. Zucchetti^{1,*}, A. Ballabio¹, D. Chrastina¹, S. Cecchi^{1,2}, M. Finazzi¹, M. Virgilio³, G. Isella¹ and F. Bottegoni¹

¹*LNES-Dipartimento di Fisica, Politecnico di Milano, Piazza Leonardo da Vinci 32, 20133 Milano, Italy*

²*Paul-Drude-Institut für Festkörperelektronik, Hausvogteiplatz 5-7, D-10117 Berlin, Germany*

³*Dipartimento di Fisica E. Fermi, Università di Pisa, Largo Pontecorvo 3, 56127 Pisa, Italy*

 (Received 26 November 2019; revised manuscript received 22 February 2020; accepted 24 February 2020; published 9 March 2020)

We investigate spin transport in a set of Ge/Si_{0.15}Ge_{0.85} multiple quantum wells (MQWs) as a function of the well thickness. We exploit optical orientation to photogenerate spin-polarized electrons in the discrete energy levels of the well conduction band at the Γ point of the Brillouin zone. After diffusion, we detect the optically oriented spins by means of the inverse spin-Hall effect (ISHE) taking place in a thin Pt layer grown on top of the heterostructure. The employed spin injection/detection scheme is sensitive to in-plane spin-polarized electrons, therefore, by detecting the ISHE signal as a function of the photon energy, we evaluate the spin polarization generated by optical transitions driven by the component of the light wave vector in the plane of the wells. In this way, we also gain insight into the electron spin-diffusion length in the MQWs. The sensitivity of the technique to in-plane spin-related properties is a powerful tool for the investigation of the in-plane component of the spin polarization in MQWs, which is otherwise commonly inaccessible.

DOI: [10.1103/PhysRevB.101.115408](https://doi.org/10.1103/PhysRevB.101.115408)

Group-IV semiconductors offer the opportunity of exploiting spin-related phenomena in platforms that are compatible with mainstream Si-based technology [1–4]. Among them, germanium allows for long spin-diffusion lengths [5–8] and efficient injection [9] and detection of spin-polarized electrons either in Ge itself [10,11] or in Ge-based heterostructures [12]. The investigation of Ge-based multiple quantum wells (MQWs), owing to the reduction of the dimensionality, adds characteristic features. Indeed, the removal of the inversion symmetry at surfaces or interfaces causes Rashba [13] or Rashba-Edelstein [14] effects to appear. Moreover, quantum confinement and strain effects cause the removal of the degeneracy between heavy-hole (HH) and light-hole (LH) states at the Γ point of the Brillouin zone, which is of particular interest for optical orientation [15,16]. Indeed, this allows a fully polarized spin population to be generated at the Γ point of the conduction band of the well [17] upon the absorption of circularly polarized photons. In the case of Ge/SiGe MQWs this population preserves its spin character over long timescales [18].

It is worth noting that, differently from bulk systems, in MQWs the unit vector of the spin polarization \mathbf{u}_p is not parallel to the light wave vector \mathbf{k} [16]. This can be seen either as due to the symmetry reduction in a low-dimensional system or as a consequence of the different probabilities for optical transitions excited by circularly polarized electric fields projected normally to the in-plane or the out-of-plane component of the light wave vector \mathbf{k} [19]. Since many spin-based devices (e.g., magnetic tunnel junctions, read heads of hard-disk drives) make use of in-plane magnetization [20], and since the Rashba-Edelstein effect [13,14] depends only on

the in-plane spin component of the carriers, the knowledge of in-plane spin polarization P_{\parallel} would be especially important. However, while it is usually quite simple to directly address the spin polarization P_{\perp} generated by a light beam impinging out of plane on the MQWs [17,18], technical problems in the illumination and the detection process make it rather difficult to have access to P_{\parallel} (generated by optical transitions driven by the in-plane component of \mathbf{k}). A possible solution of this issue requires the exploitation of planar waveguides based on MQWs [21,22], which, however, would need to be engineered to be polarization insensitive. Here, we demonstrate that a Pt/MQW structure can be employed to directly infer from experimental measurement the dependence of the electron spin polarization P_{\parallel} on the incident photon energy, and thus to determine the effect of the in-plane component of the light wave vector \mathbf{k} on spin-related properties.

In this paper, we investigate the spin transport in Ge/SiGe MQWs for different well thicknesses. Spin-polarized electrons are photogenerated in the discrete conduction levels at the Γ point of Ge wells by exploiting the optical orientation technique [15,16,23]. Within 100 fs, electrons are scattered to the L valleys [24], preserving their spin polarization [18]. They then diffuse towards a thin Pt film grown on top of the MQW structure, since the L states are not well confined. Inside Pt, they are subject to the inverse spin-Hall effect (ISHE) [25,26], i.e., to a spin-dependent scattering which transforms the optically injected spin current density \mathbf{j}_s into a charge current density \mathbf{j}_c . Following the phenomenological ISHE relation [3], we have

$$\mathbf{j}_c = \gamma \mathbf{j}_s \times \mathbf{u}_p, \quad (1)$$

with γ being the efficiency of the spin-to-charge conversion, usually indicated as the spin-Hall angle. We use Pt as a spin detector due to the large γ value ($\gamma_{\text{Pt}} \approx 0.1$ [27–31]).

*carlo.zucchetti@polimi.it

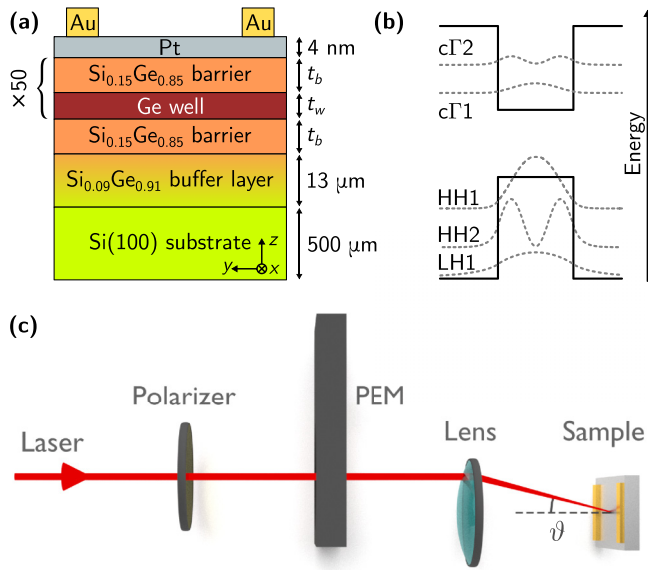


FIG. 1. Samples and experimental geometry. (a) Sketch of the samples. Symbols t_b and t_w represent the thickness of the barrier and the well, respectively, which vary from sample to sample. The spin generation occurs inside the Ge well. Spins are then transferred to the Pt layer. We acquire the electric signal due to spin-to-charge conversion in Pt between two Au contacts. (b) Sketch of the energy levels mostly contributing to optical transitions. Gray dashed lines represent the modulus squared of the wave functions corresponding to the energy levels. (c) Experimental setup.

It is worth noting that the employed spin injection/detection scheme is completely free from ferromagnetic materials, which simplifies the fabrication and makes the device intrinsically robust against external magnetic fields. The ISHE signal is measured under open circuit conditions as a voltage drop ΔV_{ISHE} across two electrodes placed at the edges of the Pt film. Since in this configuration ΔV_{ISHE} is sensitive only to the in-plane component of the spin polarization normal to the contact direction (P_x) [32–34], we show in the following that the investigation of the ISHE signal as a function of the impinging photon energy allows the spectral dependence of P_{\parallel} to be addressed. Notably, our experimental findings

are in agreement with tight-binding calculations. This points towards the exploitation of such a spin injection/detection scheme for directly accessing spin-related properties which are not otherwise accessible using common spin polarization measurement techniques.

In Fig. 1(a) we report the structure of the investigated samples. We employ the low-energy plasma-enhanced chemical vapor deposition technique to grow high-quality group-IV heterostructures [35]. On a 500- μm -thick Si(100) substrate, we grow a buffer graded from pure Si to fully relaxed $\text{Si}_{0.09}\text{Ge}_{0.91}$ with a grading rate of 7%/ μm and a 2- μm constant composition layer (total thickness: 13 μm). This serves as a virtual substrate for the growth of the first $\text{Si}_{0.15}\text{Ge}_{0.85}$ barrier of the Ge quantum well. Then, we grow 50 periods of Ge wells and $\text{Si}_{0.15}\text{Ge}_{0.85}$ barriers, with well and barrier thicknesses as reported in Table I. The structure is then terminated with a 4-nm-thick Pt layer, on which we deposit two Au contacts for the acquisition of the electric signal. Au and Pt are grown by e -beam evaporation. The direction along the electrodes [y axis in Fig. 1(a)] is parallel to the [110] crystallographic direction of the MQWs. In the following, we name the samples A–D, characterized by different barrier (t_b) and well (t_w) thickness values, as reported in Table I. The table also shows that there is a good agreement between the energy of the direct optical transitions [a sketch of the discrete energy levels is shown in Fig. 1(b)] that we extrapolate from photoreflectance measurements (see the Supplemental Material for details [36]) and the results obtained from tight-binding calculations (see below). Notably, the photoreflectance technique is sensitive also to optical transitions between QW states with different principal quantum numbers, which are barely visible in transmission [37], making it a better benchmark for tight-binding calculations.

To theoretically estimate the energy-resolved absorption coefficient and the initial optical polarization spectrum, we used a first-neighbor tight-binding (TB) Hamiltonian description of our Ge/SiGe MQW samples [39,40]. The semiempirical parametrization adopted in our model uses $sp^3d^5s^*$ orbitals in both spin configurations, and the values of the associated TB parameters for the Si and Ge crystals have been taken from Refs. [41,42], respectively. The SiGe barriers have been described by a linear interpolation of the Si and Ge

TABLE I. From the left to the right: Relevant geometrical parameters of the investigated MQW samples, t_w and t_b being the thickness of the well and the barrier, respectively, as extrapolated from X-ray diffraction measurements [37,38] (see Supplemental Material for details [36]), energies of the optical transitions between discrete levels around the direct Ge gap, as extracted from the fitting of photoreflectance measurements (see Supplemental Material for further information [36]), and, in square brackets, the results of tight-binding calculations.

Sample	t_w (nm)	t_b (nm)	HH1 \rightarrow c Γ 1 (meV)	HH2 \rightarrow c Γ 1 (meV)	LH1 \rightarrow c Γ 1 (meV)	HH3 \rightarrow c Γ 1 (meV)	HH1 \rightarrow c Γ 2 (meV)	HH2 \rightarrow c Γ 2 (meV)
A	10.7	14.8	902 [900]	913 [930]	936 [934]	974 [974]	1016 [1023]	1045 [1053]
B	12.8	17.7	889 [886]	907 [909]	918 [918]	950 [944]	981 [985]	1004 [1007]
C	14.6	20.1	879 [878]	902 [896]	915 [909]	924 [924]	956 [960]	977 [978]
D	16.1	22.1	872 [873]	892 [889]	906 [903]	927 [914]	947 [947]	954 [962]

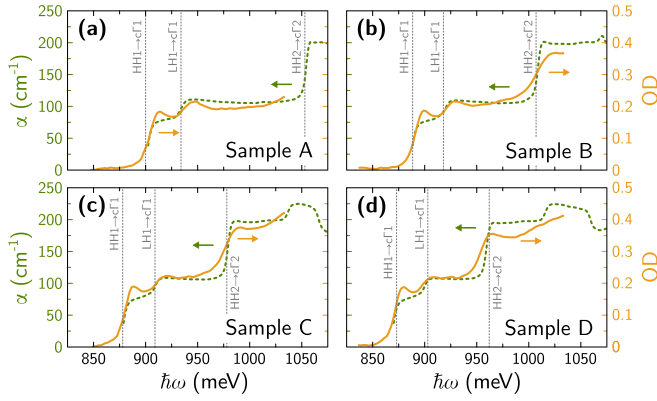


FIG. 2. Calculated absorption coefficient (α , green dotted line) and measured optical density (OD, orange continuous line) as a function of the photon energy for samples A–D [reported in (a)–(d), respectively]. Vertical gray dotted lines show the calculated energies of the main optical transitions.

parameters. Finally, since the parametrization of Refs. [41,42] holds at low temperature, a rigid shift of -90 meV of the conduction bands has been applied to take into account the temperature-induced band-gap shrinkage. Following the procedure outlined in Ref. [43], the dipole matrix elements have been expressed in terms of the hopping Hamiltonian parameters and of the first-neighbor ion positions in the strained lattice. To calculate the spectrally resolved absorption coefficient and the optical polarization spectrum, the Ge/SiGe MQW Brillouin zone has been sampled in the neighborhood of the Γ point with a grid featuring 800 nodes. Finally, to properly take into account the effects due to the coherent superposition of the doubly degenerate final states in the conduction band, the spin polarization along an arbitrary direction, induced by circularly polarized light propagating in the QW region with a given incidence angle, has been calculated as the expectation value of the density matrix operator, as reported in Ref. [16].

In Fig. 1(c) we show the experimental setup that we employ for the ISHE measurements. Electron spins are optically oriented using the monochromatized light (typical bandwidth of 10 meV) of a supercontinuum laser [44]. The circular polarization of the light beam is modulated at 50 kHz by a photoelastic modulator (PEM) [32,33]. Within the reference frame of Fig. 1(a), the Ohmic contacts can detect a current density \mathbf{j}_c parallel to the y axis. The spin current density \mathbf{j}_s flows from the MQW to the Pt layer, thus it is directed along the z axis [32–34]. Hence, Eq. (1) imposes that ΔV_{ISHE} is sensitive only to the x component of the spin polarization P_x (i.e., P_{\parallel}). To obtain a significant P_x , the light beam illuminates the samples in an off-normal configuration. This is obtained by partially filling off-axis a 0.65 numerical aperture objective [11,45–47]. The light is focused on the sample at a polar angle of $\vartheta \approx 30^\circ$, resulting in a polar angle inside the Ge layer of $\vartheta_{\text{Ge}} \approx 6.6^\circ$, almost constant within the investigated photon energy range. The ISHE signal is then extracted with a lock-in amplifier by demodulating the voltage drop across the electrodes at the PEM frequency. All measurements have been performed at room temperature.

In Fig. 2 we compare, for all the investigated samples, the absorption coefficient $\alpha(\hbar\omega)$ resulting from the

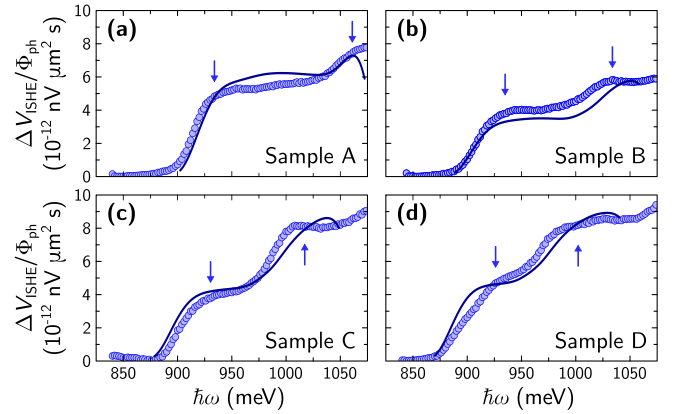


FIG. 3. Experimental results (blue circles) of ΔV_{ISHE} normalized to the photon flux Φ_{ph} for samples A–D [in (a)–(d), respectively]. The experimental error of the measurement is within the size of the circles. The dark lines represent fits of the Spicer-like model [Eq. (2)], and is proportional to $P_x \alpha$ (calculated). The light blue arrows are placed close to the absorption edges of the MQWs.

calculation (green dotted line) with the measured optical density (OD) of the MQWs (orange continuous line). The measured OD is defined as $-\log_{10}[T_S(\hbar\omega)/T_R(\hbar\omega)]$, where $T_S(\hbar\omega)$ is the transmission spectrum of the MQW sample and $T_R(\hbar\omega)$ that of a reference substrate which, in our case, consists in a $\text{Si}_{0.09}\text{Ge}_{0.91}$ relaxed buffer grown on Si. The calculated absorption coefficient nicely matches the experimental measurement. The slight difference between the two is related to excitonic absorption peaks that we do not account for in our calculations. In any case, the comparison between predicted and measured absorption spectra points towards the reliability of our theoretical approach.

In Fig. 3 we report the value of ΔV_{ISHE} normalized to the flux of the incident photons Φ_{ph} . For all the samples we can identify two shoulders, highlighted in Fig. 3 with light blue arrows. From Table I we attribute the first shoulder to the overall contribution of $\text{HH1} \rightarrow \text{c}\Gamma_1$ and $\text{LH1} \rightarrow \text{c}\Gamma_1$ transitions and the second shoulder to $\text{HH2} \rightarrow \text{c}\Gamma_2$. From sample A to sample D the energy difference between the two shoulders decreases, as expected, due to the increase of the well thickness. The spin-related nature of the ISHE signal is confirmed [11,32,34,47] as reported in Supplemental Material [36].

The ISHE spectra can be interpreted on the basis of a simple one-dimensional spin drift-diffusion model with the absorption coefficient α and the initial spin polarization within the QW P_x as input parameters. It is indeed found that the ΔV_{ISHE} dependence on α and P_x is expressed by the so-called Spicer-like formula [47,48] as

$$\Delta V_{\text{ISHE}}(\hbar\omega) \propto P_x(\hbar\omega) \frac{\alpha(\hbar\omega) \ell_s}{1 + \alpha(\hbar\omega) \ell_s}, \quad (2)$$

with ℓ_s being the effective spin-diffusion length of the MQWs along an out-of-plane path. Here, in order to gain insight into the spectral dependence of the ISHE signals, we compute the value of P_x resulting from the same tight-binding model employed for the estimation of α (see Fig. 2). We report in

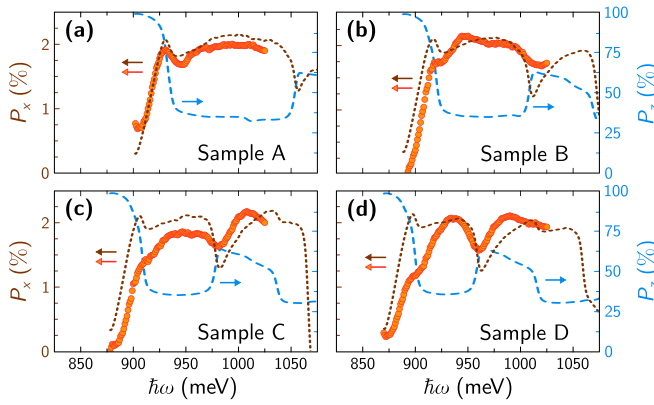


FIG. 4. In-plane (P_x , brown dotted line) and out-of-plane (P_z , light blue dashed line) component of the spin polarization as a function of the photon energy calculated for an incident angle $\vartheta_{\text{Ge}} = 6.6^\circ$ for samples A–D [respectively reported in (a)–(d)]. Red circles show the value of P_x obtained from experimental measurements as detailed in the text. Note the different spectral features of P_x and P_z due to the symmetry reduction in MQWs.

Fig. 4 the component of the spin polarization at the time of generation projected along the x and z axes [reference frame of Fig. 1(a)], P_x (brown dotted line) and P_z (light blue dashed line), respectively, calculated for $\vartheta_{\text{Ge}} = 6.6^\circ$. Since in MQWs the direction of the spin polarization \mathbf{u}_p is not parallel to the light wave vector \mathbf{k} due to symmetry reduction, it is not possible to exploit the simple definition $P_x = P \sin \vartheta_{\text{Ge}}$ and the spectral shapes of P_x and P_z (i.e., P_\perp) are different. The out-of-plane component reaches a value close to 100% for all the investigated samples, whereas P_x remains almost constant at 2% after the onset of the $\text{HH1} \rightarrow \text{c}\Gamma 1$ transitions, while a dip occurs corresponding to the $\text{HH2} \rightarrow \text{c}\Gamma 2$ transition. Here, we point out that the small absolute value of P_x is related to the small polar angle ϑ_{Ge} exploited in our experimental geometry. The tight-binding model predicts values of P_x which could reach 20% as ϑ_{Ge} approaches 90° .

The dark line in Fig. 3 shows the best fit of $\Delta V_{\text{ISHE}}/\Phi_{\text{ph}}$ obtained with the Spicer-like model [Eq. (2)]. We exploit the computed α and P_x parameters reported in Figs. 2 and 4, respectively, convoluted with a Gaussian function accounting for both the inhomogeneous broadening of the energy states and the bandwidth of the light source. The best fit for all the investigated samples yields $\Delta V_{\text{ISHE}} \propto P_x \alpha$, which means that the Spicer-like model only provides the upper constraint $\ell_s \ll \alpha^{-1}$ [see Eq. (2)]. In the investigated energy

range, the maximum value of the absorption coefficient is $\alpha \approx 200 \text{ cm}^{-1}$, hence $\ell_s \ll \alpha^{-1} \approx 50 \mu\text{m}$ for all the MQWs.

We can analyze the signal intensity to estimate a lower bound for ℓ_s . Indeed, by dividing the measured $\Delta V_{\text{ISHE}}/\Phi_{\text{ph}}$ by the electrical resistance ($R_{\text{Pt}} \approx 200 \Omega$), we obtain the value of the equivalent charge current $i_{\text{ISHE}}/\Phi_{\text{ph}}$ in the Pt layer. Then, if we assume $\gamma_{\text{Pt}} = 0.1$ [27–31], we can estimate the spin current needed to produce the detected ΔV_{ISHE} . Such a current can also be estimated directly from the Spicer-like formula [47,48]. In the limit $\ell_s \ll \alpha$ we obtain [47,48]

$$\frac{i_s}{\Phi_{\text{ph}}} = q \delta A \alpha \ell_s P_x = \frac{\Delta V_{\text{ISHE}}}{\Phi_{\text{ph}} R_{\text{Pt}} \gamma_{\text{Pt}}}, \quad (3)$$

being A the area of the spot size on the sample surface, q the elementary charge, and $\delta < 1$ a factor accounting for the presence of the Schottky barrier, which reduces the number of spins entering into Pt [47–49]. From this identity we can find the value of ℓ_s , obtaining $\ell_s \gtrsim 200 \text{ nm}$ for all the investigated samples and photon energies for vertical spin transport in Ge/SiGe MQWs. The lower bound in the estimation of ℓ_s corresponds to the case $\delta = 1$. It is worth mentioning that the range of ℓ_s we extract from our measurements is in agreement with previous estimations of the spin-diffusion length in GaAs/AlGaAs quantum wells [50,51].

Since the Spicer-like model gives $\Delta V_{\text{ISHE}} \propto P_x \alpha$ (the constant of proportionality being known from the best fit), the measurements of ΔV_{ISHE} and of the OD (properly scaled to fit the calculated α) can be used to directly estimate P_x . In Fig. 4 we report the results of this procedure. Notably, this experimentally inferred P_x value nicely agrees with the calculated values, for all the investigated samples. In particular, the comparison between the two is good for samples A and B, while, from the theoretical predictions, a slightly larger value of P_x should be expected below 925 meV for samples C and D. In any case, we can conclude that measuring ΔV_{ISHE} can directly provide information about the in-plane spin polarization, which is inaccessible to other experimental techniques.

In conclusion, we have exploited a spin injection/detection scheme in a Pt/MQW system, based on optical orientation of spin-polarized electrons in the quantum wells, and ISHE detection in the Pt layer. This yields, for all the investigated MQWs, a spin-diffusion length ℓ_s in the range between hundreds of nanometers and a few micrometers for vertical spin transport. Moreover, the sensitivity of the technique allows the in-plane spin-polarization to be experimentally estimated, which we find to be in good agreement with theoretical predictions.

- [1] J. Fabian, A. Matos-Abiague, C. Ertler, P. Stano, and I. Žutić, Semiconductor spintronics, *Acta Phys. Slovaca* **57**, 565 (2007).
- [2] D. D. Awschalom and M. E. Flatté, Challenges for semiconductor spintronics, *Nat. Phys.* **3**, 153 (2007).
- [3] M. Dyakonov, *Spin Physics in Semiconductors* (Springer, Berlin, 2008), pp. 211–244.

- [4] P. Sharma, E. Albisetti, M. Monticelli, R. Bertacco, and D. Petti, Exchange bias tuning for magnetoresistive sensors by inclusion of non-magnetic impurities, *Sensors* **16**, 1030 (2016).
- [5] C. Zucchetti, F. Bottegoni, C. Vergnaud, F. Ciccacci, G. Isella, L. Ghirardini, M. Celebrano, F. Rortais, A. Ferrari, A. Marty, M. Finazzi, and M. Jamet, Imaging spin diffusion in germanium at room temperature, *Phys. Rev. B* **96**, 014403 (2017).

- [6] F. Bottegoni, C. Zucchetti, S. Dal Conte, J. Frigerio, E. Carpena, C. Vergnaud, M. Jamet, G. Isella, F. Ciccacci, G. Cerullo, and M. Finazzi, Spin-Hall Voltage Over a Large Length Scale in Bulk Germanium, *Phys. Rev. Lett.* **118**, 167402 (2017).
- [7] K. Hamaya, Y. Fujita, M. Yamada, M. Kawano, S. Yamada, and K. Sawano, Spin transport and relaxation in germanium, *J. Phys. D: Appl. Phys.* **51**, 393001 (2018).
- [8] C. Zucchetti, M. Bollani, G. Isella, M. Zani, M. Finazzi, and F. Bottegoni, Doping dependence of the electron spin diffusion length in germanium, *APL Mater.* **7**, 101122 (2019).
- [9] J. Rioux and J. E. Sipe, Optical injection and control in germanium: Thirty-band $\mathbf{k} \cdot \mathbf{p}$ theory, *Phys. Rev. B* **81**, 155215 (2010).
- [10] J.-C. Rojas-Sánchez, M. Cubukcu, A. Jain, C. Vergnaud, C. Portemont, C. Ducruet, A. Barski, A. Marty, L. Vila, J.-P. Attané, E. Augendre, G. Desfonds, S. Gambarelli, H. Jaffrès, J.-M. George, and M. Jamet, Spin pumping and inverse spin Hall effect in germanium, *Phys. Rev. B* **88**, 064403 (2013).
- [11] C. Zucchetti, F. Bottegoni, G. Isella, M. Finazzi, F. Rortais, C. Vergnaud, J. Widiez, M. Jamet, and F. Ciccacci, Spin-to-charge conversion for hot photoexcited electrons in germanium, *Phys. Rev. B* **97**, 125203 (2018).
- [12] C. Zucchetti, M.-T. Dau, F. Bottegoni, C. Vergnaud, T. Guillet, A. Marty, C. Beigné, S. Gambarelli, A. Picone, A. Calloni, G. Bussetti, A. Brambilla, L. Duò, F. Ciccacci, P. K. Das, J. Fujii, I. Vobornik, M. Finazzi, and M. Jamet, Tuning spin-charge interconversion with quantum confinement in ultrathin bismuth films, *Phys. Rev. B* **98**, 184418 (2018).
- [13] Y. A. Bychkov and E. I. Rashba, Properties of a 2D electron gas with lifted spectral degeneracy, *JETP Lett.* **39**, 78 (1984).
- [14] V. Edelstein, Spin polarization of conduction electrons induced by electric current in two-dimensional asymmetric electron systems, *Solid State Commun.* **73**, 233 (1990).
- [15] D. T. Pierce and F. Meier, Photoemission of spin-polarized electrons from GaAs, *Phys. Rev. B* **13**, 5484 (1976).
- [16] F. Meier and B. P. Zakharchenya, *Optical Orientation* (Elsevier, Amsterdam, 1984).
- [17] F. Bottegoni, A. Ferrari, G. Isella, S. Cecchi, M. Marcon, D. Chrastina, G. Trezzi, and F. Ciccacci, Ge/SiGe heterostructures as emitters of polarized electrons, *J. Appl. Phys.* **111**, 063916 (2012).
- [18] F. Pezzoli, F. Bottegoni, D. Trivedi, F. Ciccacci, A. Giorgioni, P. Li, S. Cecchi, E. Grilli, Y. Song, M. Guzzi, H. Dery, and G. Isella, Optical Spin Injection and Spin Lifetime in Ge Heterostructures, *Phys. Rev. Lett.* **108**, 156603 (2012).
- [19] G. Bastard, *Wave Mechanics Applied to Semiconductor Heterostructures* (Wiley, New York, 1990).
- [20] T. Jungwirth, J. Wunderlich, and K. Olejník, Spin Hall effect devices, *Nat. Mater.* **11**, 382 (2012).
- [21] P. Chaisakul, D. Marris-Morini, J. Frigerio, D. Chrastina, M.-S. Rouified, S. Cecchi, P. Crozat, G. Isella, and L. Vivien, Integrated germanium optical interconnects on silicon substrates, *Nat. Photonics* **8**, 482 (2014).
- [22] M. Rouified, D. Marris-Morini, P. Chaisakul, J. Frigerio, G. Isella, D. Chrastina, S. Edmond, X. Le Roux, J. Coudeville, D. Bouville, and L. Vivien, Advances toward Ge/SiGe quantum-well waveguide modulators at 1.3 μm , *IEEE J. Sel. Top. Quantum Electron.* **20**, 33 (2014).
- [23] G. Lampel, Nuclear Dynamic Polarization by Optical Electronic Saturation and Optical Pumping in Semiconductors, *Phys. Rev. Lett.* **20**, 491 (1968).
- [24] C. Lange, G. Isella, D. Chrastina, F. Pezzoli, N. S. Köster, R. Woscholski, and S. Chatterjee, Spin band-gap renormalization and hole spin dynamics in Ge/SiGe quantum wells, *Phys. Rev. B* **85**, 241303(R) (2012).
- [25] M. Dyakonov and V. Perel, Possibility of orienting electrons spins with current, *JETP Lett.* **13**, 467 (1971).
- [26] M. Dyakonov and V. Perel, Current-induced spin orientation of electrons in semiconductors, *Phys. Lett. A* **35**, 459 (1971).
- [27] K. Ando, S. Takahashi, K. Harii, K. Sasage, J. Ieda, S. Maekawa, and E. Saitoh, Electric Manipulation of Spin Relaxation Using the Spin Hall Effect, *Phys. Rev. Lett.* **101**, 036601 (2008).
- [28] A. Azevedo, L. H. Vilela-Leão, R. L. Rodríguez-Suárez, A. F. Lacerda Santos, and S. M. Rezende, Spin pumping and anisotropic magnetoresistance voltages in magnetic bilayers: Theory and experiment, *Phys. Rev. B* **83**, 144402 (2011).
- [29] W. Zhang, V. Vlaminck, J. E. Pearson, R. Divan, S. D. Bader, and A. Hoffmann, Determination of the Pt spin diffusion length by spin-pumping and spin Hall effect, *Appl. Phys. Lett.* **103**, 242414 (2013).
- [30] M. Obstbaum, M. Härtinger, H. G. Bauer, T. Meier, F. Swientek, C. H. Back, and G. Woltersdorf, Inverse spin Hall effect in $\text{Ni}_{81}\text{Fe}_{19}$ /normal-metal bilayers, *Phys. Rev. B* **89**, 060407(R) (2014).
- [31] M. Isasa, E. Villamor, L. E. Hueso, M. Gradhand, and F. Casanova, Temperature dependence of spin diffusion length and spin Hall angle in Au and Pt, *Phys. Rev. B* **91**, 024402 (2015).
- [32] K. Ando, M. Morikawa, T. Trypiniotis, Y. Fujikawa, C. H. W. Barnes, and E. Saitoh, Direct conversion of light-polarization information into electric voltage using photoinduced inverse spin-Hall effect in Pt/GaAs hybrid structure: Spin photodetector, *J. Appl. Phys.* **107**, 113902 (2010).
- [33] F. Bottegoni, A. Ferrari, G. Isella, M. Finazzi, and F. Ciccacci, Experimental evaluation of the spin-Hall conductivity in Si-doped GaAs, *Phys. Rev. B* **88**, 121201(R) (2013).
- [34] F. Bottegoni, C. Zucchetti, F. Ciccacci, M. Finazzi, and G. Isella, Optical generation of pure spin currents at the indirect gap of bulk Si, *Appl. Phys. Lett.* **110**, 042403 (2017).
- [35] G. Isella, D. Chrastina, B. Rössner, T. Hackbarth, H.-J. Herzog, U. König, and H. von Känel, Low-energy plasma-enhanced chemical vapor deposition for strained Si and Ge heterostructures and devices, *Solid-State Electron.* **48**, 1317 (2004).
- [36] See Supplemental Material at <http://link.aps.org/supplemental/10.1103/PhysRevB.101.115408> for details about X-ray diffraction measurements, photoreflectance measurements, and additional data confirming the spin-related nature of the ISHE signal.
- [37] A. Ballabio, J. Frigerio, S. Firoozabadi, D. Chrastina, A. Beyer, K. Volz, and G. Isella, Ge/SiGe parabolic quantum wells, *J. Phys. D: Appl. Phys.* **52**, 415105 (2019).
- [38] D. Kriegner, E. Wintersberger, and J. Stangl, *xrayutilities*: A versatile tool for reciprocal space conversion of scattering data recorded with linear and area detectors, *J. Appl. Crystallogr.* **46**, 1162 (2013).
- [39] M. Virgilio, M. Bonfanti, D. Chrastina, A. Neels, G. Isella, E. Grilli, M. Guzzi, G. Grosso, H. Sigg, and H. von Känel, Polarization-dependent absorption in Ge/SiGe multiple quantum wells: Theory and experiment, *Phys. Rev. B* **79**, 075323 (2009).

- [40] M. Virgilio and G. Grosso, Quantum-confined Stark effect in Ge/SiGe quantum wells: A tight-binding description, *Phys. Rev. B* **77**, 165315 (2008).
- [41] J.-M. Jancu, R. Scholz, F. Beltram, and F. Bassani, Empirical *spds** tight-binding calculation for cubic semiconductors: General method and material parameters, *Phys. Rev. B* **57**, 6493 (1998).
- [42] J.-M. Jancu and P. Voisin, Tetragonal and trigonal deformations in zinc-blende semiconductors: A tight-binding point of view, *Phys. Rev. B* **76**, 115202 (2007).
- [43] F. Trani, G. Cantele, D. Ninno, and G. Iadonisi, Tight-binding calculation of the optical absorption cross section of spherical and ellipsoidal silicon nanocrystals, *Phys. Rev. B* **72**, 075423 (2005).
- [44] SuperK Extreme EXW-12, NKT Photonics. The laser delivers nanosecond pulses at a 78 MHz repetition rate in the 0.7–2.2 eV range. Here, we do not exploit the temporal structure of the laser source. Indeed, our results are time averaged since the temporal average of the time-dependent spin drift-diffusion equation equals the solution for the spin drift-diffusion equation in the steady state (see Ref. [49]).
- [45] M. Savoini, F. Ciccacci, L. Duò, and M. Finazzi, Apparatus for vectorial Kerr confocal microscopy, *Rev. Sci. Instrum.* **82**, 023709 (2011).
- [46] C. Stamm, C. Murer, M. Berritta, J. Feng, M. Gabureac, P. M. Oppeneer, and P. Gambardella, Magneto-Optical Detection of the Spin Hall Effect in Pt and W Thin Films, *Phys. Rev. Lett.* **119**, 087203 (2017).
- [47] F. Bottegoni, C. Zucchetti, G. Isella, M. Bollani, M. Finazzi, and F. Ciccacci, Spin-charge interconversion in heterostructures based on group-IV semiconductors, *Riv. Nuovo Cimento* **1** (2020), doi: [10.1007/s40766-020-0002-0](https://doi.org/10.1007/s40766-020-0002-0).
- [48] F. Bottegoni, C. Zucchetti, G. Isella, E. Pinotti, M. Finazzi, and F. Ciccacci, Modeling the photo-induced inverse spin-Hall effect in Pt/semiconductor junctions, *J. Appl. Phys.* **124**, 033902 (2018).
- [49] C. Zucchetti, G. Isella, F. Ciccacci, M. Finazzi, and F. Bottegoni, Spin transport and spin-charge interconversion phenomena in Ge-based structures, *Proc. SPIE* **11090**, 73 (2019).
- [50] C. Hu, H. Ye, G. Wang, H. Tian, W. Wang, W. Wang, B. Liu, and X. Marie, Room temperature spin diffusion in (110) GaAs/AlGaAs quantum wells, *Nanoscale Res. Lett.* **6**, 149 (2011).
- [51] G. Wang, B. L. Liu, A. Balocchi, P. Renucci, C. R. Zhu, T. Amand, C. Fontaine, and X. Marie, Gate control of the electron spin-diffusion length in semiconductor quantum wells, *Nat. Commun.* **4**, 2372 (2013).